LACTATE DEHYDROGENASE A-COUPLED NAD+ REGENERATION IS CRITICAL FOR ACUTE MYELOID LEUKEMIA CELL SURVIVAL

Ayşegül Erdem[1], Séléna Kaye[1], Francesco Caligiore[2], Manuel Johanns[3], Fleur Leguay[1], Jan Jacob Schuringa[4], Keisuke Ito[5], Guido Bommer[2] and Nick van Gastel[1,6]

[1]Cellular Metabolism and Microenvironment Laboratory, de Duve Institute, UCLouvain, Brussels, Belgium. [2]Biochemistry and Metabolic Research Group, de Duve Institute, UCLouvain, Brussels, Belgium. [3]Protein Phosphorylation Group, de Duve Institute, UCLouvain, Brussels, Belgium. [4]Department of Experimental Hematology, University Medical Center Groningen, University of Groningen, Groningen, The Netherlands. [5]Ruth L. and David S. Gottesman Institute for Stem Cell and Regenerative Medicine Research, Albert Einstein College of Medicine, Bronx, NY 10461, USA; Department of Cell Biology, Albert Einstein College of Medicine, Bronx, NY 10461, USA; Departments of Oncology and Medicine, Albert Einstein College of Medicine-Montefiore Health System, Bronx, NY 10461, USA. [6]WELBIO Department, WEL Research Institute, Wavre, Belgium.

Correspondance to: nick.vangastel@uclouvain.be

Key words

Cancer metabolism, Acute myeloid leukemia, Glycolysis, Lactate dehydrogenase A, Redox balance, NAD+

1

27 **Abstract**

28

29 **Background**

30 Enhanced glycolysis plays a pivotal role in fueling the aberrant proliferation, survival and

31 therapy resistance of acute myeloid leukemia (AML) cells. Here, we aimed to elucidate the

32 extent of glycolysis dependence in AML by focusing on the role of lactate dehydrogenase A

33 (LDHA), a key glycolytic enzyme converting pyruvate to lactate coupled with the recycling of

34 NAD^+.

35

36 **Methods**

37 We compared the glycolytic activity of primary AML patient samples to protein levels of

38 metabolic enzymes involved in central carbon metabolism including glycolysis, glutaminolysis

39 and the tricarboxylic acid cycle. To evaluate the therapeutic potential of targeting glycolysis in

40 AML, we treated AML primary patient samples and cell lines with pharmacological inhibitors

41 of LDHA and monitored cell viability. Glycolytic activity and mitochondrial oxygen consumption

42 were analyzed in AML patient samples and cell lines post-LDHA inhibition. Perturbations in

43 global metabolite levels and redox balance upon LDHA inhibition in AML cells were

44 determined by mass spectrometry, and ROS levels were measured by flow cytometry.

45

46 **Results**

47 Among metabolic enzymes, we found that LDHA protein levels had the strongest positive

48 correlation with glycolysis in AML patient cells. Blocking LDHA activity resulted in a strong

49 growth inhibition and cell death induction in AML cell lines and primary patient samples, while

50 healthy hematopoietic stem and progenitor cells remained unaffected. Investigation of the

51 underlying mechanisms showed that LDHA inhibition reduces glycolytic activity, lowers levels

52 of glycolytic intermediates, decreases the cellular NAD^+ pool, boosts OXPHOS activity and

53   increases ROS levels. This increase in ROS levels was however not linked to the observed

54   AML cell death. Instead, we found that LDHA is essential to maintain a correct NAD^+/NADH

55   ratio in AML cells. Continuous intracellular NAD^+ supplementation via overexpression of water-

56   forming NADH oxidase from *Lactobacillus brevis* in AML cells effectively increased viable cell

57   counts and prevented cell death upon LDHA inhibition.

58

59   **Conclusions**

60   Collectively, our results demonstrate that AML cells critically depend on LDHA to maintain an

61   adequate NAD^+/NADH balance in support of their abnormal glycolytic activity and biosynthetic

62   demands, which cannot be compensated for by other cellular NAD^+ recycling systems. These

63   findings also highlight LDHA inhibition as a promising metabolic strategy to eradicate leukemic

64   cells.

65

66

67

68

69

70

71

72

73

74

75

76

77

78

79 **Background**

80

81 Acute myeloid leukemia (AML) is a heterogeneous hematological malignancy characterized

82 by the rapid growth of abnormal myeloid progenitor cells in the bone marrow, leading to

83 impaired hematopoiesis [1, 2]. Despite therapeutic advances, patients continue to experience

84 poor outcomes and high rates of relapse, highlighting the need for a more profound

85 understanding of the molecular mechanisms that drive leukemogenesis.

86

87 Since the initial observations of Otto Warburg regarding the reliance of cancer cells on aerobic

88 fermentation for their energy production [3], extensive research over more then a century has

89 underscored the importance of metabolic abnormalities in cancer development. Yet, the

90 complex relationship between disrupted cellular metabolism and oncogenic progression has

91 only started to become elucidated. Emerging evidence indicates that dysregulated metabolism

92 not only fuels the aberrant proliferation and survival of AML tumors [4], but also plays a pivotal

93 role in chemoresistance [5-9]. While metabolic profiles can differ significantly between AML

94 patients and even within AML tumors [10-12], glycolysis has been shown to be essential for

95 AML blasts in most patient populations, distinguishing itself from other metabolic pathways by

96 providing rapid ATP production, crucial biosynthetic precursors, and an adaptive advantage

97 in the hypoxic bone marrow microenvironment [13, 14]. In accordance, the glycolytic

98 metabolites lactate and pyruvate are elevated in AML patient serum samples [15]. Additionally,

99 interactions with the bone marrow microenvironment enhance glycolysis in AML cells, with

100 this glycolytic shift being regulated by the CXCL12/CXCR4/mTOR signaling axis, which serves

101 as a protective mechanism against chemotherapy [16]. Pyruvate dehydrogenase kinase

102 (PDK) enzymes, which inhibit the entrance of pyruvate into the mitochondrial tricarboxylic acid

103 (TCA) cycle, have been shown to fine-tune glycolysis by suppressing mitochondrial oxidative

104 phosphorylation (OXPHOS) not only in leukemic blasts [10], but also in leukemia-initiating

4

105   cells (also known as leukemic stem cells; LSCs) [13]. LSCs, while generally considered to

106   depend more on OXPHOS, thus also require a functional glycolytic pathway, and this further

107   increases when AML cells are treated with OXPHOS inhibitors [17, 18]. Despite the overall

108   importance of glycolysis in AML, the role of individual glycolytic enzymes has been explored

109   much less in depth. A better characterization of the differential dependency of AML cells on

110   specific glycolytic enzymes could offer new therapeutic opportunities.

111

112   Lactate dehydrogenase A (LDHA), a predominant enzyme in aerobic and anaerobic

113   glycolysis, plays a pivotal role in supporting the energetic and biosynthetic demands of cancer

114   cells. By catalyzing the conversion of pyruvate to lactate, LDHA facilitates the regeneration of

115   nicotinamide adenine dinucleotide (NAD^+), thereby promoting glycolytic flux and maintaining

116   redox balance. As such, LDHA also diverts glucose-derived pyruvate away from other

117   metabolic fates, such as entry into the mitochondrial TCA cycle for further oxidation or

118   conversion into alanine. In the context of AML, dysregulated LDHA activity has been

119   implicated in leukemogenesis and disease progression, highlighting its potential as a

120   therapeutic target. A pioneering study by Wang *et al.* showed that loss of the glycolytic

121   enzymes PKM2 (pyruvate kinase isoform M2) and LDHA has different effects on healthy and

122   leukemic hematopoietic stem and progenitor cells (HSPCs) in mice [19]. While loss of PKM2,

123   which lowers but does not block glycolytic flux, negatively affects hematopoietic progenitor

124   cells (HPCs) and AML cells, hematopoietic stem cells (HSCs) are spared. Complete inhibition

125   of fermentation by loss of LDHA in contrast equally impacts HSCs, HPCs and AML cells.

126   However, while the effects of LDHA loss in HSCs could be ascribed to increased mitochondrial

127   respiration and associated reactive oxygen species (ROS) generation, the role of LDHA in

128   AML cells was independent of ROS buffering capacity and remains unknown. The importance

129   of LDHA for human AML cells has also not yet been explored.

130

131 Considering the differential importance and regulation of glycolysis in healthy and malignant

132 hematopoiesis, a better understanding of the specific roles of individual glycolytic enzymes is

133 needed to design therapeutic strategies that target AML cells while maximally sparing their

134 non-malignant counterparts. Here, we set out to explore the mechanistic interplay between

135 LDHA-mediated metabolism and human AML pathophysiology by dissecting the direct cellular

136 and molecular consequences of LDHA inhibition in AML primary patient samples and cell lines.

137

138

139

140

141

142

143

144

145

146

147

148

149

150

151

152

153

154

155

156

Results

Human AML cells are sensitive to LDHA enzyme inhibition

To better understand the role of individual enzymes in the regulation of glycolytic activity in AML cells, we re-analyzed our previously generated data [10] and correlated protein levels of central carbon metabolism enzymes (including those involved in glycolysis, the TCA cycle and glutaminolysis) of primary AML patient blasts (n=13; CD34+ fraction, or total mononuclear cells in case of NPM1 mutant AML) with their glycolytic activity as measured by the extracellular acidification rate (ECAR). Pearson [10] correlation analysis showed that LDHA protein levels had the highest positive correlation with ECAR activity in the patient blasts (Fig. 1A). Protein levels of pyruvate dehydrogenase phosphatase 1 (PDP1), which promotes shuttling of pyruvate towards the TCA cycle, was found to have the most negative correlation with the ECAR response (Fig. 1A). To validate this observation, we treated different human AML cell lines (n=5) and primary patient blasts (CD34+ cells, n=3) with a number of widely used inhibitors related to lactate/pyruvate metabolism: AZD3965 (an inhibitor of the lactate transporter monocarboxylate transporter 1; MCT1), Compound 3k (an inhibitor of PKM2, which regulates the final and rate-limiting step of glycolysis by converting phosphoenolpyruvate to pyruvate) and FX11 (an inhibitor of LDHA). We found that AML cells were highly sensitive to FX11 compared to the other two inhibitors whereby FX11 treatment also showed comparable susceptibility across different AML subtypes (Fig. 1C, Supplementary Table 1). To confirm this, we treated a range of human AML cell lines with FX11 or an unrelated selective LDHA inhibitor (GSK2837808A) and measured both viable cell numbers and the percentage of dead cells 48 hours later. In all cell lines tested, and for both LDHA inhibitors, a strong induction of cell death was observed (Fig. 1D-G). We also treated a panel of AML primary patient blasts (n=12; CD34+ fraction, or total mononuclear blasts in case of CD34- AMLs; see Supplementary Table 1) with the two LDHA inhibitors for 48 hours and

183   found a reduced number of viable cells upon LDHA inhibition across samples (Fig. 1H). To

184   check possible toxic effects of LDHA inhibition on healthy HSPCs, we tested cord blood-

185   derived CD34+ cells (n=3 different donors), which did not show any signs of cell death after 48

186   hours of treatment with 20μM FX11 (Fig. 1I, J). These data underscore the importance of

187   LDHA for maintaining the viability of AML cells and indicate the existence of a differential

188   dependency on this metabolic enzyme compared to healthy HSPCs.

189

190   **LDHA inhibition reduces glycolysis and increases OXPHOS activity in AML cells**

191   To investigate the metabolic consequences of LDHA inhibition, we monitored glycolysis and

192   mitochondrial OXPHOS activity in AML cells by respectively measuring the ECAR and oxygen

193   consumption rate (OCR) using extracellular flux analysis (Seahorse assay). Cells were first

194   exposed to either of the two LDHA inhibitors, followed by injection of glucose, oligomycin (to

195   inhibit mitochondrial ATP synthase) and 2-DG (2-deoxyglucose; a glucose analog and

196   upstream inhibitor of glycolysis) into the culture medium. NB4 and HL60 cells showed a

197   significantly lower ECAR and higher OCR after 10 minutes of LDHA inhibition, indicating a

198   reduction in glycolytic activity (Fig. 2A-D) and a compensatory increase in OXPHOS (Fig. 2E,

199   F). We confirmed this observation in several primary AML patient blasts (AML4, AML6,

200   AML11; see Fig. 1H and Supplementary Table 1) that, when pre-treated with GSK2837808A,

201   significantly reduced their ECAR and increased the OCR (Fig. 2G, H). This suggests that

202   pharmacological LDHA inhibition reverses the Warburg effect and boosts oxidative

203   phosphorylation in AML cells.

204

205   **Increased ROS levels after LDHA inhibition are not responsible for the observed AML**

206   **cell death**

207   In a previous study in mice, it was shown that loss of LDHA in HSCs increases ROS levels

208   because of increased OXPHOS activity, and these excessive ROS levels disrupt HSC

8

209   maintenance [19]. However, AML cell death upon loss of LDHA could not be clearly linked to

210   ROS. We therefore wondered whether LDHA inhibition in human AML cells would augment

211   ROS levels due to increased OXPHOS activity, and could cause the observed cell death. We

212   measured ROS levels in AML cell lines (n=8) by flow cytometry using a CellROX dye after

213   exposing the cells to increasing concentrations of FX11 for 24 hours. ROS levels were

214   significantly increased up to 5-fold as compared to control samples (Fig. 3A). Since the

215   antioxidant N-acetyl-L-cysteine (NAC) has been reported to decrease ROS in HSCs [19], we

216   performed a rescue experiment by supplementing NAC post-LDHA inhibition to understand if

217   excess ROS contributes to AML cell death. Interestingly, although NAC supplementation

218   reduced ROS nearly to control levels (Fig. 3B), cell viability was not rescued upon LDHA

219   inhibition (Fig. 3C). As an independent approach, we also co-cultured AML cells with bone

220   marrow derived mesenchymal stromal cells (MS-5 cell line) that were previously shown to

221   reduce ROS levels in AML cells [20]. Similar to our above-mentioned results with NAC

222   supplementation, MS-5 co-cultures significantly reduced ROS levels (Fig. 3D) but cell viability

223   after LDHA inhibition was not rescued (Fig. 3E). Similar results were obtained with primary

224   AML patient samples (Supplementary Fig. 1A). Collectively, these findings suggest that

225   excessive ROS levels induced by LDHA inhibition are not the main cause of cell death in AML

226   cells.

227

228   **Global metabolic changes induced in AML cells after LDHA inhibition**

229   To further define the metabolic status of AML cells after LDHA inhibition, we measured

230   intracellular metabolites after 15 minutes and 24 hours of treatment with FX11, assessing

231   short-term and long-term consequences respectively. Metabolites were extracted from 3

232   different AML cell lines and analyzed by liquid chromatography-coupled mass spectrometry

233   (LC-MS). After normalization of the samples to the internal standard (d8-valine), we

234   investigated common changes occurring in the 3 AML cell lines across different metabolic

235   pathways, including glycolysis, the pentose phosphate pathway (PPP), hexosamine

236   biosynthesis, the TCA cycle and redox balance after 24 hours (Fig. 4A). Several upstream

237   glycolytic metabolites such as hexose, glucose-6-phosphate and fructose-6-phosphate were

238   significantly reduced after 15 minutes and 24 hours of treatment with FX11 (Fig. 4B) in AML

239   cells. Expectedly, intracellular lactate levels were significantly reduced after FX11 treatment

240   in NB4 cells (Fig. 4C), which was further confirmed across different AML cell lines

241   (Supplementary Fig. 1B, n=3), showing reduced pyruvate fermentation to lactate.

242

243   Besides the effect on glycolysis, treatment of AML cells with FX11 for 24 hours reduced the

244   levels of several PPP metabolites, while changes in hexosamine biosynthesis (Fig. 4A) and in

245   amino acids (Supplementary Fig.1C) were less evident. When examining the levels of TCA

246   cycle metabolites, we found an overall reduction across the different cell lines after FX11

247   treatment (Fig. 4A). The reason for this was unclear, given the increase in OCR in AML cells

248   treated with LDHA inhibitors (Fig. 2E, F). To further examine this, we measured the

249   mitochondrial membrane potential of AML cells (n=8) exposed to increasing doses of FX11,

250   which confirmed higher OXPHOS activity (Supplementary Fig. 1D). Additional experiments

251   revealed that this increase in membrane potential was associated with an increase in lipid

252   uptake (Supplementary Fig. 1E), suggesting that AML cells may increase fatty acid oxidation

253   in response to inhibition of glycolysis, resulting in higher OXPHOS activity.

254

255   Both glycolysis and OXPHOS can be used by cells for ATP generation to meet bioenergetic

256   demands. To assess whether the observed increase in OXPHOS was sufficient to

257   compensate for reduced glycolytic activity upon LDHA inhibition in AML cells, we measured

258   phosphorylation of 5' AMP-activated protein kinase (AMPK), which acts as a key cellular

259   energy sensor. In all cell lines tested we detected increased AMPK phosphorylation in the

260   presence of FX11 (Fig. 4D), indicating that even though OXPHOS activity increases, AML

261 cells critically depend on LDHA to maintain their energy balance. Additional supplementation

262 of cells with different anaplerotic substrates, including pyruvate, glutamine or a cell-permeable

263 form of 2-oxoglutarate, to increase the levels of TCA cycle intermediates could however not

264 prevent the induction of cell death by LDHA inhibition (Supplementary Fig. 1F), showing that

265 the lower levels of TCA cycle metabolites are not responsible for the observed cell death.

266

267 Given the importance of glycolysis and the PPP in regulating the cellular redox status, we next

268 looked more carefully at the levels of NADH, NAD^+, NADPH, $NADP^+$, reduced glutathione

269 (GSH), oxidized glutathione (GSSG) and their respective ratios. In line with the role of LDHA

270 in regenerating NAD^+ from NADH, we found increased levels of NADH, decreased levels of

271 NAD^+ and a decreased NAD^+/NADH ratio in FX11-treated AML cells at both early and later

272 time points (Fig. 4E, F). We also found decreased levels of NADPH relative to $NADP^+$ and

273 higher GSSG versus GSH levels (Fig. 4F), in line with a decreased PPP activity and increased

274 demand for ROS detoxification (see Fig. 3). Since we already ruled out increased ROS as the

275 reason for LDHA inhibition-induced AML cell death, we next focused on the role of LDHA in

276 maintaining the cytosolic NAD^+/NADH ratio.

277

278 **LDHA is essential to maintain the intracellular NAD^+/NADH balance in AML cells**

279 LDHA catalyzes the interconversion of pyruvate and lactate with concomitant interconversion

280 of reduced NADH and NAD^+. In glycolysis, LDHA ferments pyruvate to lactate and thereby

281 regenerates NAD^+, an essential co-factor for the central glycolytic enzyme glyceraldehyde 3-

282 phosphate dehydrogenase (GAPDH). Given this role of LDHA and the stable decline in NAD^+

283 levels in different AML cell lines post-LDHA inhibition (Fig. 5A), we decided to further study

284 the consequences of the disturbance in intracellular NAD^+/NADH balance. We first validated

285 our metabolomics results with an independent approach by monitoring the cytosolic

286 NAD^+/NADH ratio using a genetically-encoded fluorescent biosensor. Peredox-mCherry was

287 designed with a bacterial NADH-binding protein linked to a circularly permuted green

288 fluorescent T-Sapphire and a NADH-insensitive red fluorescent mCherry, allowing

289 measurement of the cytosolic free NAD^+/NADH ratio as the red-to-green fluorescence ratio

290 [21, 22]. We transduced NB4 cells (a glycolytic and LDHA inhibitor-sensitive AML cell line)

291 with a Peredox-mCherry encoding lentiviral vector and sorted mCherry$^+$ cells. When these

292 cells were treated for 15 minutes with either FX11 or GSK2837808A, an increase in the green

293 fluorescent signal (FITC channel) relative to mCherry signal was detected by flow cytometry

294 (Fig. 5B), confirming that LDHA inhibition decreases the NAD^+/NADH ratio.

295

296 To test whether the reduced NAD^+/NADH ratio was responsible for cell death induction upon

297 LDHA inhibition in AML cells, we tested whether re-balancing the NAD^+/NADH ratio could

298 rescue AML cell death. To this end, we transduced NB4 cells with lentiviral constructs

299 overexpressing a mitochondrial or cytosolic variant of the water-forming NADH oxidase (NOX)

300 from *Lactobacillus brevis* (*Lb*NOX) [23]. Quantification of intracellular NAD^+ levels using a

301 colorimetric assay showed that stable expression of either mitochondria- or cytosol-targeted

302 *Lb*NOX increased cellular NAD^+ levels compared to control cells and normalized NAD^+ levels

303 in NB4 cells treated with GSK2837808A (Fig. 5C) or FX11 (Fig. 5D) which was also reflected

304 in the NAD^+/NADH ratios (Supplementary Fig.1 G, H). Analysis of AML cell death post-LDHA

305 inhibition with GSK2837808A or FX11 showed that restoration of cellular NAD^+ levels by

306 *Lb*NOX significantly reduced cell death, although it was not fully prevented (Fig. 5E, F). In

307 accordance, cell viability was significantly higher in *Lb*NOX-overexpressing cells compared to

308 controls when treated with increasing doses of GSK2837808A or FX11 (Fig. 5G, H).

309 Collectively, these findings show that LDHA plays a direct and central role in maintaining the

310 NAD^+/NADH balance in AML cells (Figure 5I, upper panel), and that the absence of this

311 enzyme leads to a metabolic imbalance that cannot be compensated for by other enzymes,

312 ultimately triggering cell death in AML cells (Figure 5I, lower panel).

Discussion

AML blasts display a typical Warburg metabolism with high rates of aerobic glycolysis supporting the bioenergetic and biosynthetic demands of increased proliferation, redox regulation, hyperactive signaling cascades and therapy-induced damage repair [10, 13, 15, 19]. Unlike certain solid tumor types, where the role of individual glycolytic enzymes and their therapeutic potential has been studied in detail [24], a good strategy for targeting glycolytic metabolism in AML cells has remained elusive. In the current study, we showed that among glycolytic enzymes LDHA protein levels show the highest correlation with glycolytic activity in AML cells, and that LDHA inhibition shows potent anti-leukemic effects in both AML cell lines and primary patient samples, while sparing non-malignant hematopoietic cells. We further found that inhibition of LDHA impacts AML cell viability by lowering the cellular NAD^+/NADH ratio, leading to reduced ATP generation through glycolysis that cannot be compensated for by increased mitochondrial OXPHOS activity.

One of the first studies revealing the dependence of AML blasts on aerobic glycolysis was that of Wang *et al.*, where they showed that loss of either PKM2 or LDHA enforced a metabolic shift from glycolysis to mitochondrial respiration and strongly inhibited leukemia initiation and maintenance in mice [19]. Although the effects of PKM2 deletion on normal hematopoiesis were relatively mild *in vivo*, HSCs from $Ldha^{-/-}$ mice exhibited increased ROS levels that negatively affected their functioning. However, depletion of LDHA did not impair the ROS buffering capacity of AML cells, suggesting distinct effects of LDHA loss on normal and malignant HSPCs. In line with their observation, we found that excessive ROS levels resulting from LDHA inhibition in human AML cells were not responsible for the observed cell death. Instead, in AML cells LDHA is key to maintain an optimal cytosolic NAD^+/NADH ratio that allows maximal glycolytic flux and prevents cell death. In contrast to the Wang *et al.* study,

13

339   where mouse HSCs, HPCs and AML cells were all shown to be equally impacted by complete

340   loss of LDHA, we found that normal human HSPCs are less sensitive to LDHA inhibitors

341   compared to AML blasts. As indicated by our extracellular flux (Fig. 2) and metabolomics (Fig.

342   4) analysis, the concentrations of LDHA inhibitors that we used in our study decrease but do

343   not completely shut down LDHA activity, suggesting the existence of a therapeutic window,

344   where partial inhibition of LDHA kills leukemic but not healthy HSPCs.

345

346   In the current study we focus on bulk AML cells, but recent findings from us and others shows

347   that LSCs, or at least a subset of them, also depend on a high glycolytic flux. Using the

348   genetically encoded metabolic sensor SoNar, which like Peredox reports the cytosolic

349   NADH/NAD$^+$ ratio, it was shown that cells with high cytosolic NADH/NAD$^+$ ratios are highly

350   glycolytic, enriched for LSCs, and reside in the hypoxic endosteal niche in an MLL-AF9-driven

351   model of mouse AML [13]. In this model, pyruvate dehydrogenase kinase 2 (PDK2) was found

352   to be essential for preventing pyruvate entry into the mitochondria and maintaining glycolytic

353   activity and LSC properties. In our own previous work in human AML, we found that PDK1^{high}

354   AMLs are highly glycolytic, have low OXPHOS and are enriched for stemness signatures [10].

355   In addition, these AMLs are mostly wildtype for FLT3 and NPM1, in contrast to FLT3-ITD and

356   NPM1^c AMLs that are OXPHOS-dependent [10, 11]. It will be of interest to explore the

357   therapeutic potential of LDHA inhibitors in future *in vivo* studies, for example using patient-

358   derived AML xenografts harboring different genetic mutations, to test the efficacy of LDHA

359   inhibitors in eradicating LSCs with high glycolytic signatures, investigate the effects in AMLs

360   carrying metabolically-distinct subclones and study potential escape mechanisms.

361

362   An important finding of our study is that LDHA is absolutely essential for maintaining the

363   optimal NAD$^+$/NADH ratio in AML cells, and that this function cannot by compensated for by

364   other endogenous NAD$^+$ regenerating systems such as the malate-aspartate shuttle or the

365 glycerol-3-phosphate shuttle that move glycolysis-derived NADH into the mitochondria for

366 oxidation. Indeed, inhibition of LDHA increased the OCR and mitochondrial membrane

367 potential while lowering the levels of TCA cycle metabolites, which may indicate that excessive

368 shuttling of cytosolic NADH to the mitochondria for oxidation leads to inhibition of NAD^+-

369 dependent TCA cycle reactions. In accordance, both cytosolic and mitochondrial forms of

370 *Lb*NOX rescued cellular NAD^+/NADH ratios and viability, indicating that while NADH shuttling

371 systems in AML cells are very active, increased activity of complex I of the electron transport

372 chain cannot prevent a drop in the NAD^+/NADH ratio when LDHA activity is reduced. Other

373 NAD^+ regenerating systems, such as NAD^+ synthesis and salvage pathways, also do not seem

374 to be able to compensate for the loss of LDHA. Tumor cells have been shown to increase

375 NAD^+ levels and upregulate NAD^+ synthesis and salvage enzyme expression to support redox

376 homeostasis and to fulfil the high demands of proliferation [25]. It has been recently noted that

377 depleting NAD^+ by inhibiting nicotinamide phosphoribosyltransferase (NAMPT), a key enzyme

378 in the NAD^+ salvage pathway, offers a therapeutical window in AML [26]. In LDHA-dependent

379 lymphoma models, combinatory treatment of NAMPT inhibition and the LDHA inhibitor FX11

380 induced tumor regression in *in vivo* xenograft models [27]. In addition, a recent study

381 highlighted that dual inhibition of the NADPH oxidase NOX2 and glycolysis —by targeting

382 hexokinase or LDH— significantly reduced cell proliferation and delayed leukemia progression

383 [28]. These findings, together with our current results, underscore the importance of redox

384 metabolism to meet the particular bioenergetic, biosynthetic and antioxidant demands of AML

385 cells. With this in mind, future studies should aim to further dissect the mechanisms by which

386 genetically-distinct AMLs meet their redox demands and how this metabolic rheostat is

387 impacted by different therapies. In addition, it will be worth to investigate if and how AML blasts

388 and LSCs can adapt to different therapies impacting NAD^+ pools or the NAD^+/NADH balance.

389 In this context, targeting LDHA holds promise in AML as it hits the Warburg effect at its core,

390   shows a therapeutic window compared to healthy HSPCs and cannot be prevented by the

391   presence of bone marrow stromal cells, which often protect AML cells from therapies.

392

393

394

395

396

397

398

399

400

401

402

403

404

405

406

407

408

409

410

411

412

413

414

415

Methods

Ex vivo AML and healthy primary cell cultures and *in vitro* cell culture conditions

Human AML cell lines (THP1, HL60, NB4, Mono-Mac-6 [MM6], MV411, NOMO1, MOLM14, OCIAML3 and U937, all from DSMZ) used in this study were maintained in RPMI-1640 medium (Gibco) supplemented with 10% fetal bovine serum (FBS, Sigma-Aldrich), 2 mM glutamine (ThermoFisher Scientific) and 1% antibiotics mix composed of penicillin and streptomycin (P/S; ThermoFisher Scientific). Cell line identity was validated by DNA fingerprinting. CD34$^+$ human cord blood-derived cells were obtained from STEMCELL Technologies and were maintained in StemSpan SFEM-II with CD34 supplements (STEMCELL Technologies).

Primary AML specimens (CD34$^+$ cells and mononuclear cells for CD34$^-$ samples) were obtained after written informed consent at the Montefiore Medical Center/Montefiore Einstein Comprehensive Cancer Center (for patient characteristics see Supplementary Table 1). Frozen bone marrow aspirates were thawed in a water bath at 37 °C and resuspended in alpha-Minimum Essential Medium (α-MEM, ThermoFisher Scientific) supplemented with 2% FBS, DNase I (20 Units/mL), 4 mM $MgSO_4$ and heparin (5 Units/mL) and incubated at 37 °C for 15 minutes. Primary AML cells were plated in Gartner's medium consisting of α-MEM supplemented with 12.5% heat-inactivated FBS (Sigma-Aldrich), 12.5% heat-inactivated horse serum (Invitrogen), 1% P/S, 57.2 μM β-mercaptoethanol (Sigma-Aldrich) and 1 mM hydrocortisone (Sigma-Aldrich), with the addition of G-CSF (Amgen), N-Plate (Clinical grade TPO; Amgen) and IL-3 (Sandoz) (all 20 ng/mL). For AML cell line co-cultures, mouse bone marrow derived MS-5 stromal cells (DSMZ) were expanded in α-MEM with GlutaMAX, 10% FBS and 1% P/S, plated in culture flasks and expanded to form a confluent layer, to which AML cells were added. Liquid cultures and co-cultures were grown at 37 °C and 5% CO_2.

442

443   We used HEK-293T cells to produce lentiviral particles, which were cultured in Dulbecco's

444   Modified Eagle's Medium (D-MEM) (high glucose, ThermoFisher Scientific) supplemented

445   with 10% FBS, 2 mM glutamine and 1% P/S.

446

447   **Reagents**

448   Reagents purchased include: FX11 (HY-16214, Bio-connect), GSK2837808A (HY-100681,

449   Bio-connect), AZD3965 (HY-12750, Bio-connect), Compound 3k (HY-103617, Bio-connect),

450   N-acetyl-L-cysteine (NAC; A9165, Sigma-Aldrich). For flow cytometric reagents see section

451   below, and Seahorse reagents are indicated in Seahorse assay section.

452

453   **Flow cytometry and sorting procedures**

454   Cell death was quantified by Annexin V staining (FITC) according to manufacturer's protocol

455   (#560931, BD Biosciences). Equal number of cells were stained with Annexin V in calcium-

456   supplied sterile water buffer for 20 minutes at 4 °C in the dark followed by DAPI staining for

457   10 minutes. CellROX Orange (C10443, ThermoFisher Scientific) was used at 1 μM final

458   concentration in phosphate-buffered saline (PBS) for 15 minutes in the dark at 37°C. BODIPY-

459   FL-C$_{16}$ (4,4-Difluoro-5,7-Dimethyl-4-Bora-3a,4a-Diaza-s-Indacene-3-Hexadecanoic Acid,

460   D3821, ThermoFisher Scientific; a green fluorescent fatty acid used to measure lipid uptake)

461   was used at 1 μM final concentration in PBS for 15 minutes in the dark at 37 °C. MitoTracker

462   Deep Red (M46753, ThermoFisher Scientific) was used at 500 nM final concentration in PBS

463   for 15 minutes in the dark at 37°C. Analysis was performed on a FACSVerse system (BD

464   Biosciences).

465

466   For monitoring the cytosolic NADH/NAD$^+$ ratio, NB4 cells were lentivirally transduced with the

467   NADH-sensitive Peredox probe under the control of a phosphoglycerate kinase (PGK)

468   promoter [21]. After transduction, mCherry+ cells were sorted (FACSAria II; BD Biosciences).

469   NADH-sensitive green fluorescence (FITC channel; mean fluorescence intensity) was

470   recorded by flow cytometry (FACSVerse; BD Biosciences) and expressed relative to stable

471   mCherry mean fluorescence intensity, before and after the treatment with FX11 for 15 minutes.

472   The mCherry/FITC ratio therefore indicates changes in NAD+/NADH ratio. Results were

473   analyzed using the FlowJo Software (BD Biosciences).

474

475   **Liquid Chromatography-coupled Mass Spectrometry (LC-MS)**

476   1×10^6 AML cells were collected after 24 hours of treatment with 20 μM FX11 and washed with

477   sterile UltraPure DNase/RNase-Free Distilled Water (10977049, Life Technologies Europe).

478   Cells were maintained on ice during the process to keep their metabolism stabilized. For the

479   extraction, 200 μL of 9:1 Methanol/Chloroform (#1.06035 and #650471, Sigma-Aldrich),

480   supplemented with 5 μM D8-valine (DLM-311-1, Buchem BV; internal standard) was added to

481   the cells. Samples were vortexed and centrifuged at 13 000 rpm at 4 °C for 10 minutes.

482   Supernatant was harvested and dried down with a SpeedVac machine for 2 hours

483   approximately. Samples were stored at -80 °C until the LC-MS analysis was conducted. Right

484   before the analysis, 45 μL of 80% methanol in water was added to the samples. From that, 30

485   μL was loaded in an LC-MS vial and untargeted LC-MS analysis was performed as previously

486   described [29]. Briefly, 5 μL of sample was injected and separated on an Inertsil 3 μm particle

487   ODS-4 column (150 x 2.1 mm; GL Biosciences) at a constant flow rate of 0.2 mL/min with an

488   Agilent 1290 HPLC system. Mobile phase A consisted of 5 mM hexylamine (Sigma-Aldrich)

489   adjusted to pH 6.3 with acetic acid (Biosolve BV) and phase B of 90% methanol (Biosolve

490   BV)/10% 10 mM ammonium acetate (Biosolve BV) adjusted to pH 8.5 with ammonia (Merck).

491   The mobile phase profile consisted of the following steps and linear gradients: 0 – 2 min at

492   0% B; 2 – 6 min from 0 to 20% B; 6 – 17 min from 20 to 31% B; 17 – 36 min from 31 to 60%

493   B; 36 – 41 min from 60 to 100% B; 41 – 51 min at 100% B; 51 – 53 min from 100 to 0% B; 53

494 – 60 min at 0% B. Analytes were identified with an Agilent 6550 ion funnel mass spectrometer

495 operated in negative mode with an electrospray ionization (ESI) source and the following

496 settings: ESI spray voltage 3500 V, sheath gas 350 °C at 11 L/min, nebulizer pressure 35 psig

497 and drying gas 200 °C at 14 L/min. An m/z range from 70 to 1200 was acquired with a

498 frequency of 1 per second by adding 8122 transients. Compound identification was based on

499 their exact mass (<5 ppm) and retention time compared to standards. The areas under the

500 curve of extracted-ion chromatograms of the [M-H]$^-$ forms were integrated using MassHunter

501 software (Agilent, Santa Clara, CA, USA), and normalized to the mean of the areas obtained

502 for a series of 150 other metabolites ('total ion current'). Metabolites were further characterized

503 in MS2 by fragmentation with 10, 20 and 40 V and 150 ms acquisition time per spectrum and

504 a 4 mass unit isolation window.

505

506 **Seahorse assay**

507 Oxygen consumption rate (OCR) and Extra Cellular Acidification Rate (ECAR) were measured

508 using a Seahorse XF96 analyzer (Seahorse Bioscience, Agilent, US) at 37 °C. For AML cell

509 lines 100.000 cells and for primary AML samples 200.000 cells were seeded per well in poly-

510 L-lysine (Sigma-Aldrich) coated Seahorse XF96 plates in 180 μL XF Assay Medium (Modified

511 DMEM, Seahorse Bioscience). For OCR measurements, XF Assay Medium was

512 supplemented with 10 mM Glucose and 20 μM of FX11 or 10 μM of GSK2837808A (Port A),

513 2.5 μM oligomycin A (Port B), 2.5 μM FCCP (carbonyl cyanide-4-[trifluorometh oxy]

514 phenylhydrazone) (Port C) and 2 μM antimycin A together with 2 μM Rotenone (Port D) were

515 sequentially injected to measure basal and maximal OCR levels (all reagents from Sigma-

516 Aldrich). For ECAR measurements, Glucose-free XF Assay medium was added to the cells

517 and 20 μM of FX11 or 10 μM of GSK2837808A (Port A), 10 mM Glucose (Port B), 2.5 μM

518 oligomycin A (Port C) and 100 mM 2-deoxy-D-glucose (Port D) were sequentially injected (all

519 reagents from Sigma-Aldrich). The XF96 protocol consisted of 4 times mix (2 minutes) and

520   measurement (2 minutes) cycles, allowing for determination of OCR/ECAR at baseline and in

521   between injections. Both basal and maximal OCR levels as well as basal ECAR and glycolytic

522   capacity measurements were calculated by assessing metabolic response of the cells in

523   accordance with the manufacturer's instructions. The OCR and ECAR measurements were

524   normalized to the number of cells used for the assay. Seahorse Wave Desktop software

525   (Agilent) was used to design assays and for data analysis.

526

527   **Lentiviral vectors and transduction**

528   Cytosol-directed or mitochondria-directed *Lb*NOX (*Lactobacillus brevis* NADH oxidase)

529   lentiviral constructs were provided by Dr. Jakub Rohlena (Czech Academy of Sciences) and

530   were made by PCR amplifying *Lb*NOX or mito-*Lb*NOX cDNAs from the original pUC57 vectors

531   (#75285, #74448, Addgene), cleaving the cDNAs with fast digest EcoRI and BamHI restriction

532   enzymes(ThermoFisher Scientific) and ligated them into EcoRI and BamHI-cleaved pCDH-

533   CMV-MCS-EF-puro lentiviral plasmids. Correct insertion was verified by sequencing.

534   Lentiviruses were generated in HEK293T cells using empty vectors, cyto-*Lb*NOX or mito-

535   *Lb*NOX (4 μg plasmid) together with 3 μg of delta 8.9 packaging plasmid and 2 μg of vesicular

536   stomatitis virus (VSV-G) envelope plasmid using the Fugene transfection system (Promega,

537   Madison, USA). After 48 hours, viral supernatant was harvested, filtered through a 0.45 μm

538   filter, and used to transduce recipient cells (with 8 μg/mL polybrene to increase the infection

539   efficiency). Cells were cultured in the presence of 1 μg puromycin for selection after

540   transduction. The lentiviral vector containing the peredox probe was previously generated [21].

541   Briefly, the pcDNA3.1-Peredox-mCherry plasmid was obtained from the Addgene collection

542   (plasmid #32383) and Peredox-mCherry was subcloned using a Gateway strategy into

543   pTM978 (*PGK*>Gateway-IRES-Neo). Lentiviruses were generated as above.

544

545   **NAD$^+$/NADH assay**

21

546 Intracellular $NAD^+/NADH$ ratios were measured using a $NAD^+/NADH$ Quantitation kit (Sigma-

547 Aldrich, MAK460) which allows to measure both total NAD^+ and NADH levels in the cells.

548 1×10^6 NB4 cells were seeded in culture plates for each condition, and the assay was

549 performed after 24 hours of incubation with either 20 μM FX11 or GSK. We used equal protein

550 amount (20 μg) of each sample (in technical duplicates or triplicates) in 96 well plates and

551 recorded fluorescence using a GloMax® Discover spectrophotometer (Promega). We then

552 calculated NAD^+ and NADH levels using a standard curve and following the manufacturer's

553 instructions.

554

555 **Western blot**

556 Cell pellets from AML cell lines (1×10^6 cells) were lysed in RIPA buffer (#89900,

557 ThermoFisher Scientific) supplemented with protease inhibitors (cOmplete Mini;

558 #11836153001, Sigma-Aldrich) and phosphatase inhibitors (PhosSTOP, #4906837001,

559 Sigma-Aldrich), and were sonicated in an ice bath at 25 kHz, power 100 for 1 minute. Lysates

560 were then boiled at 100 °C for 5 minutes in 4x Laemmli sample Buffer (#1610747, Bio-Rad)

561 containing 10% β-mercaptoethanol (M3148, Sigma-Aldrich). We loaded 25 μg of proteins/well

562 into 4–15% mini–Protean TGX precast gels for SDS-PAGE (#4561085, Bio-Rad) and

563 transferred proteins to 0.45 μm low fluorescence PVDF membranes (Trans-Blot Turbo RTA

564 Mini Transfer kit, #1704274, Bio-Rad). Membranes were blocked in 5% BSA (A9418, Sigma-

565 Aldrich) in Tris-buffered saline (TBS) 1X and incubated for 1 hour at room temperature on a

566 rotary shaker. Then, membranes were incubated overnight with primary antibodies prepared

567 in 5% BSA in TBS at 1:1000 dilution (rabbit anti-AMPK [2532S, Cell Signaling]: rabbit anti-

568 phosphoAMPK [2535S, Cell Signaling]) + 1:50000 of mouse anti-actin (A5441, Sigma-Aldrich)

569 used as a loading control. After several washes with TBS 1x + Tween 0.1% (TBST) (P1379,

570 Sigma-Aldrich), secondary antibodies were added, prepared in 5% milk in TBS 1X; 1:30000

571 for actin (goat anti-mouse secondary antibody coupled with Dylight680; #35518,

572   ThermoFisher Scientific) and 1:15000 for the test antibodies (goat anti-rabbit secondary

573   antibody coupled with Dylight800, #SA-35571, ThermoFisher Scientific) . The membrane was

574   placed on the shaker, in the dark, at room temperature for 1 hour. After, we washed the

575   membranes 3 times for 5 minutes with TBST and 2 times for 5 minutes with TBS. An Odyssey

576   XF Imager (LICORbio) was used to scan and analyze the membranes.

577

578   **Statistical analysis**

579   All statistical analysis was performed using the GraphPad Prism Software. The means were

580   plotted with errors bars representing standard error of the mean (SEM) with a minimal of 3

581   technical replicates and at least 3 biological replicates, unless otherwise indicated in the figure

582   legend. Two-tailed student's t-test were used to calculate the statistical significance between

583   two groups, one-way ANOVA was used to calculate the statistical significance between three

584   groups or more with one experimental parameter and two-way ANOVA for two or more

585   experimental parameters. We chose an interval of confidence at 95% and the p-value was

586   considered statistically significant if inferior to 0.05. For the figures, * = p-value < 0.05, ** = p-

587   value < 0.01 and *** = p- value < 0.001.

588

589

590

591

592

593

594

595

596

597

References

1. Ley, T.J., et al., *Genomic and epigenomic landscapes of adult de novo acute myeloid leukemia.* N Engl J Med, 2013. **368**(22): p. 2059-74.

2. Miller, C.A., R.K. Wilson, and T.J. Ley, *Genomic landscapes and clonality of de novo AML.* N Engl J Med, 2013. **369**(15): p. 1473.

3. Warburg, O., *Über den Stoffwechsel der Carcinomzelle.* Naturwissenschaften, 1924. **12**: p. 1131-1137.

4. Mishra, S.K., S.E. Millman, and L. Zhang, *Metabolism in acute myeloid leukemia: mechanistic insights and therapeutic targets.* Blood, 2023. **141**(10): p. 1119-1135.

5. Jones, C.L., et al., *Inhibition of Amino Acid Metabolism Selectively Targets Human Leukemia Stem Cells.* Cancer Cell, 2018. **34**(5): p. 724-740.e4.

6. Jones, C.L., et al., *Nicotinamide Metabolism Mediates Resistance to Venetoclax in Relapsed Acute Myeloid Leukemia Stem Cells.* Cell Stem Cell, 2020. **27**(5): p. 748-764.e4.

7. Ye, H., et al., *Leukemic Stem Cells Evade Chemotherapy by Metabolic Adaptation to an Adipose Tissue Niche.* Cell Stem Cell, 2016. **19**(1): p. 23-37.

8. van Gastel, N., et al., *Induction of a Timed Metabolic Collapse to Overcome Cancer Chemoresistance.* Cell Metab, 2020. **32**(3): p. 391-403.e6.

9. Farge, T., et al., *Chemotherapy-Resistant Human Acute Myeloid Leukemia Cells Are Not Enriched for Leukemic Stem Cells but Require Oxidative Metabolism.* Cancer Discov, 2017. **7**(7): p. 716-735.

10. Erdem, A., et al., *The Glycolytic Gatekeeper PDK1 defines different metabolic states between genetically distinct subtypes of human acute myeloid leukemia.* Nat Commun, 2022. **13**(1): p. 1105.

11. Erdem, A., et al., *Inhibition of the succinyl dehydrogenase complex in acute myeloid leukemia leads to a lactate-fuelled respiratory metabolic vulnerability.* Nat Commun, 2022. **13**(1): p. 2013.

12. de Boer, B., et al., *Prospective Isolation and Characterization of Genetically and Functionally Distinct AML Subclones.* Cancer Cell, 2018. **34**(4): p. 674-689.e8.

13. Hao, X., et al., *Metabolic Imaging Reveals a Unique Preference of Symmetric Cell Division and Homing of Leukemia-Initiating Cells in an Endosteal Niche.* Cell Metab, 2019. **29**(4): p. 950-965.e6.

14. Yang, Y., J. Pu, and Y. Yang, *Glycolysis and chemoresistance in acute myeloid leukemia.* Heliyon, 2024. **10**(15).

15. Chen, S., et al., *Glucose induced-AKT/mTOR activation accelerates glycolysis and promotes cell survival in acute myeloid leukemia.* Leukemia Research, 2023. **128**: p. 107059.

16. Braun, M., et al., *CXCL12 promotes glycolytic reprogramming in acute myeloid leukemia cells via the CXCR4/mTOR axis.* Leukemia, 2016. **30**(8): p. 1788-1792.

17. Baccelli, I., et al., *Mubritinib Targets the Electron Transport Chain Complex I and Reveals the Landscape of OXPHOS Dependency in Acute Myeloid Leukemia.* Cancer Cell, 2019. **36**(1): p. 84-99 e8.

18. Molina, J.R., et al., *An inhibitor of oxidative phosphorylation exploits cancer vulnerability.* Nat Med, 2018. **24**(7): p. 1036-1046.

19. Wang, Y.-H., et al., *Cell-State-Specific Metabolic Dependency in Hematopoiesis and Leukemogenesis.* Cell, 2014. **158**(6): p. 1309-1323.

20. Forte, D., et al., *Bone Marrow Mesenchymal Stem Cells Support Acute Myeloid Leukemia Bioenergetics and Enhance Antioxidant Defense and Escape from Chemotherapy.* Cell Metab, 2020. **32**(5): p. 829-843.e9.

673   21.   Johanns, M., et al., *Inhibition of basal and glucagon-induced hepatic glucose production by 991 and other pharmacological AMPK activators.* Biochemical Journal, 2022. **479**(12): p. 1317-1336.

676   22.   Masia, R., et al., *Live cell imaging of cytosolic NADH/NAD+ ratio in hepatocytes and liver slices.* American Journal of Physiology-Gastrointestinal and Liver Physiology, 2018. **314**(1): p. G97-G108.

679   23.   Titov, D.V., et al., *Complementation of mitochondrial electron transport chain by manipulation of the NAD^{+}/NADH ratio.* Science, 2016. **352**(6282): p. 231-235.

682   24.   Stine, Z.E., et al., *Targeting cancer metabolism in the era of precision oncology.* Nat Rev Drug Discov, 2022. **21**(2): p. 141-162.

684   25.   Yong, J., S. Cai, and Z. Zeng, *Targeting NAD+ metabolism: dual roles in cancer treatment.* Frontiers in Immunology, 2023. **14**.

686   26.   Subedi, A., et al., *Nicotinamide phosphoribosyltransferase inhibitors selectively induce apoptosis of AML stem cells by disrupting lipid homeostasis.* Cell Stem Cell, 2021. **28**(10): p. 1851-1867.e8.

689   27.   Le, A., et al., *Inhibition of lactate dehydrogenase A induces oxidative stress and inhibits tumor progression.* Proceedings of the National Academy of Sciences, 2010. **107**(5): p. 2037-2042.

692   28.   Ijurko, C., et al., *Targeting NOX2 and glycolytic metabolism as a therapeutic strategy in acute myeloid leukaemia.* Biomarker Research, 2024. **12**(1): p. 128.

694   29.   Heremans, I.P., et al., *Parkinson's disease protein PARK7 prevents metabolite and protein damage caused by a glycolytic metabolite.* Proc Natl Acad Sci U S A, 2022. **119**(4).

697

698

699 **Figure Legends**

700

701 **Figure 1. Human AML cells are sensitive to LDHA inhibition.**

702 **A**. Pearson correlation of protein levels of central carbon metabolism enzymes involved in

703 glycolysis, the TCA cycle and glutaminolysis of primary AML patient blasts (n=13) versus their

704 glycolytic activity as measured by the extracellular acidification rate (ECAR) (data retrieved

705 from Erdem *et al.* [10]). **B**. Correlation of LDHA protein expression compared to ECAR activity

706 of CD34$^+$ AML primary samples ($n=13$). **C**. Heatmap showing fold change in number of viable

707 (DAPI$^-$) AML cells (n=5 cell lines, n=3 AML primary patient samples) 24 hours after treatment

708 with FX11 (20 μM), AZD3965 (4 μM) or Compound 3k (5 μM). **D-E**. Number of viable (DAPI$^-$)

709 cells relative to the controls in AML cells following 20 μM FX11 (D) or 20 μM GSK2837808A

710 (E) treatment for 24 hours. Each dot represents a biological replicate measured in technical

711 triplicate. **F-G**. Percentage dead (Annexin V$^+$DAPI$^+$) AML cells upon 20 μM FX11 (F) or 20 μM

712 GSK2837808A (G) treatment for 24 hours. Each dot represents a biological replicate

713 measured in technical triplicate. **H**. Number of viable (DAPI$^-$) cells relative to controls in AML

714 primary patient samples following 20 μM FX11 or 20 μM GSK2837808A treatment for 48

715 hours. Each dot represents a technical replicate. **I-J**. Number of viable (DAPI$^-$) cells relative to

716 controls (I) and percentage dead (Annexin V$^+$DAPI$^+$) (J) healthy cord blood-derived CD34$^+$

717 cells following 20 μM FX11 or 20 μM GSK2837808A treatment for 48 hours. Each dot

718 represents a biological replicate measured in technical triplicate. **B**: linear regression analysis;

719 **D,E,F,G,I,J**: one-way ANOVA; **H**: two-way ANOVA for multiple comparisons. All experiments:

720 lines and error bars represent mean ± SEM. *$p < 0.05$; **$p < 0.01$; ***$p < 0.001$; ****$p < 0.0001$;

721 ns, not significant.

722

723

28

Figure 2. Inhibiting LDHA decreases glycolytic activity while promoting oxidative phosphorylation in AML cells.

A-B. Real-time extracellular acidification rate (ECAR) of AML cell lines NB4 (A) and HL60 (B) (mean ± SEM of biological triplicates) measured by Seahorse bioassay after sequential injections of either of the two LDHA inhibitors (20 μM of FX11, 10 μM of GSK2837808A), glucose, oligomycin and 2-DG. **C-F**. Bar graphs showing glycolytic capacity (C: FX11, D: GSK2837808A) and maximal oxygen consumption rate (OCR; E: FX11, F: GSK2837808A) of NB4 and HL60 AML cells. **G-H**. Basal ECAR (G) and OCR (H) after pre-treatment of AML primary patient samples (n=3, each dot represents a technical replicate) with 10 μM GSK2837808A. **G**,**H**: Student's t-test; **C,D,E,F**: one-way ANOVA; **A,B**: two-way ANOVA for multiple comparisons. All experiments: bars and error bars represent mean ± SEM. *$p < 0.05$; **$p < 0.01$; ***$p < 0.001$; ns, not significant.

Figure 3. Increased ROS levels do not contribute to AML cell death following LDHA inhibition.

A. Heatmap showing the fold change of CellROX Orange mean fluorescent intensity in AML cell lines exposed to increasing concentrations of FX11 for 24 hours, compared to DMSO treated controls. Data show mean of biological triplicates. **B**. Fold change (FC) of CellROX Orange mean fluorescent intensity (MFI) in AML cell lines exposed to 20 μM FX11 in the presence and absence of NAC (N-acetyl-L-cysteine, 2 mM) for 24 hours. Each dot represents a biological replicate measured in technical triplicate. **C**. Number of viable (DAPI⁻) cells relative to controls in AML cells (each dot represents a distinct AML cell line, as mean of biological replicates) following 20 μM FX11 treatment in the presence and absence of 2 mM NAC for 24 hours. **D**. Fold change of CellROX Orange mean fluorescent intensity in AML cell lines exposed to 20 μM FX11 in the presence (co-culture) and absence (mono-culture) of MS-5 cells for 24 hours. Each dot represents a biological replicate measured in technical triplicate.

750 **E**. Number of viable (DAPI⁻) cells relative to controls in AML cells (each dot represents a

751 distinct AML cell line, as mean of biological replicates) following 20 μM FX11 treatment in the

752 presence and absence of MS-5 cells for 24 hours. **B,C,D,E**: one-way ANOVA; **A**: two-way

753 ANOVA for multiple comparisons. All experiments: bars and error bars represent mean ± SEM.

754 *$p < 0.05$; **$p < 0.01$; ***$p < 0.001$; ****$p < 0.0001$.

755

756 **Figure 4. LDHA inhibition induces global metabolic changes.**

757 **A.** Heatmap showing metabolomics results of AML cells (n=3) after 24 hours of treatment with

758 20 μM FX11. Data show mean of technical triplicates as fold change compared to vehicle-

759 treated groups. **B-C**. Glycolysis-related metabolites (B) and intracellular lactate abundance

760 (C) in NB4 cells after 15 minutes and 24 hours of treatment with 20 μM FX11, as measured

761 by LC-MS (each dot represents a biological replicate). **D**. Western blot for p-AMPK and AMPK

762 in AML cells lines grown for 24 hours in the presence or absence of 20 μM FX11. β-actin was

763 used as loading control. Image shown is a representative of three independent replicates. **E**.

764 NAD⁺/NADH ratio in NB4 AML cells after 15 minutes and 24 hours of treatment with 20 μM

765 FX11, as measured by LC-MS (each dot represents a biological replicate). **F**. Relative

766 abundance of redox homeostasis related metabolites in NB4 cells after 15 minutes and 24

767 hours of treatment with 20 μM FX11, as measured by LC-MS (each dot represents a biological

768 replicate). **B,C,E,F**: one-way ANOVA. All experiments: bars and error bars represent mean ±

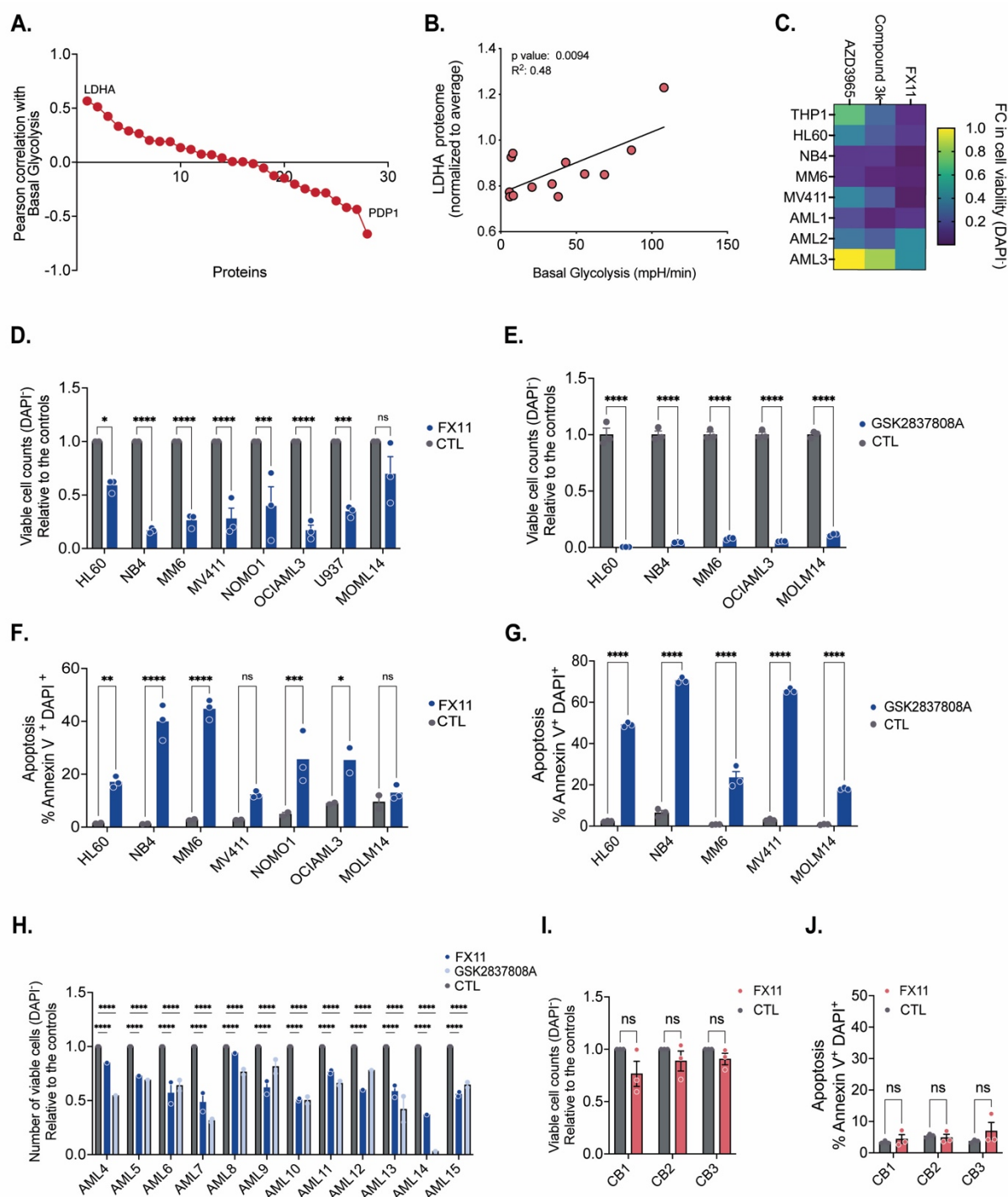769 SEM. *$p < 0.05$; **$p < 0.01$; ***$p < 0.001$.

770

771 **Figure 5. LDHA critically regulates the intracellular NAD⁺/NADH ratio in AML cells**

772 **A**. Intracellular NAD⁺ abundance in AML cell lines after 24 hours of treatment with 20 μM

773 FX11, as measured by LC-MS (n=4 technical replicates). **B**. Red (insensitive to NADH)-to-

774 green (sensitive to NADH) fluorescence ratio in Peredox-mCherry-expressing NB4 cells

775 treated for 15 minutes with either FX11 or GSK2837808A. Each dot represents a biological
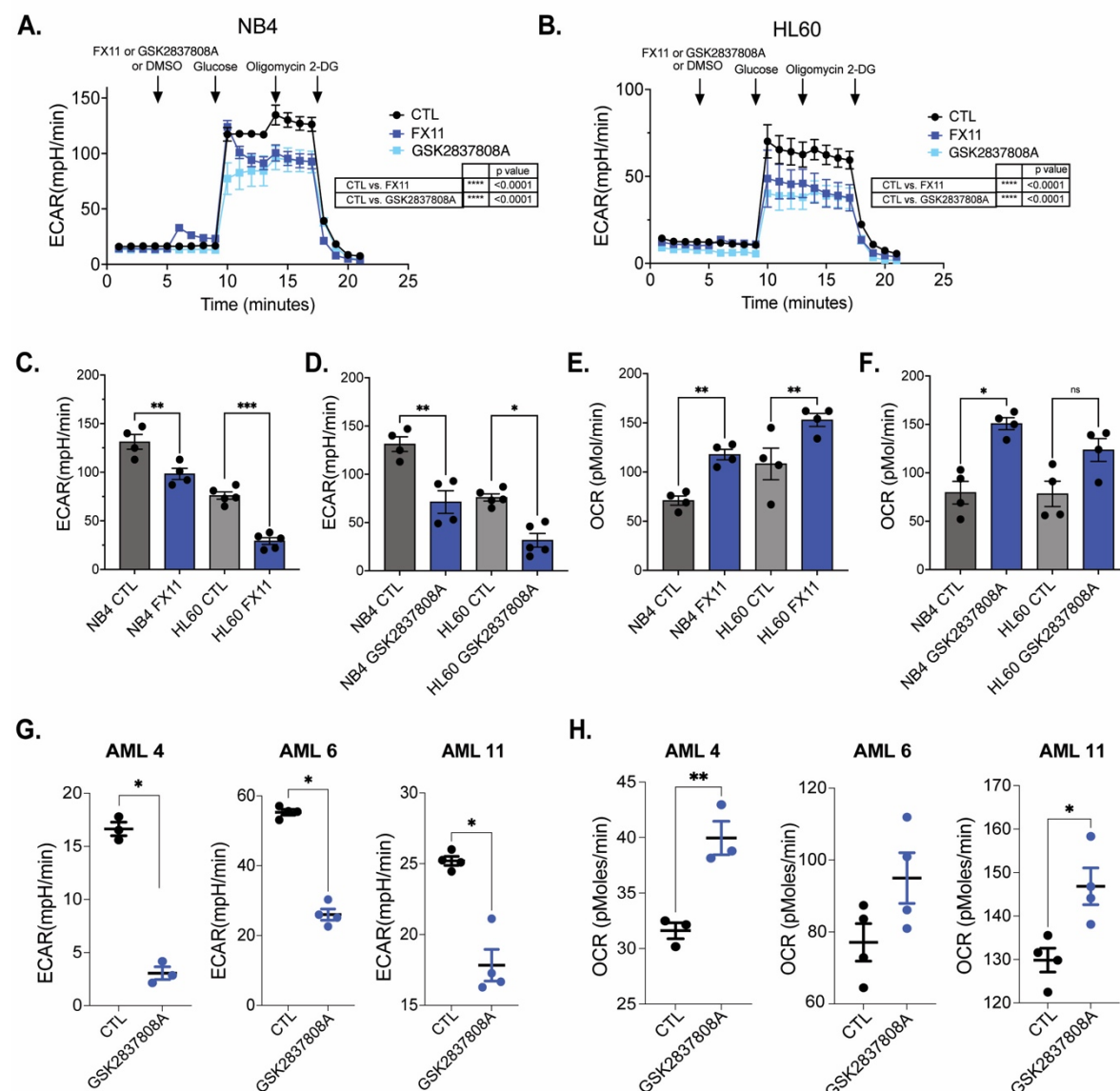
776   replicate. **C-D**. Cellular NAD$^+$ levels in NB4 control cells, NB4 cells transduced with an empty

777   vector (EV) and NB4 cells overexpressing a mitochondrial or cytosolic variant of *Lb*NOX,

778   treated with vehicle or 20 μM GSK2837808A (C) or 20 μM FX11 (D) for 24 hours, as measured

779   by enzymatic assay. **E-F**. Percentage dead (Annexin V$^+$DAPI$^+$) NB4 control cells, NB4 cells

780   transduced with an EV and NB4 cells overexpressing a mitochondrial or cytosolic variant of

781   *Lb*NOX, treated with vehicle or 20 μM GSK2837808A (E) or 20 μM FX11 (F) for 24 hours. **G-**

782   **H**. Percentage live (Annexin V$^-$DAPI$^-$) NB4 control cells, NB4 cells transduced with an EV and

783   NB4 cells overexpressing a mitochondrial or cytosolic variant of *Lb*NOX, treated with

784   increasing doses of GSK2837808A (G) or FX11 (H) for 18 hours. **I**. Graphical abstract

785   depicting the metabolic role of LDHA in AML cells (upper panel) and consequences of LDHA

786   inhibition (lower panel). G-6-P = Glucose 6-phosphate, F-6-P = Fructose 6- phosphate, F-1,6-

787   BP = Fructose 1,6-bisphosphate. **A-F**: one-way ANOVA; **G,H**: two-way ANOVA for multiple

788   comparisons. All experiments: bars and error bars represent mean ± SEM. *$p < 0.05$; **$p <$

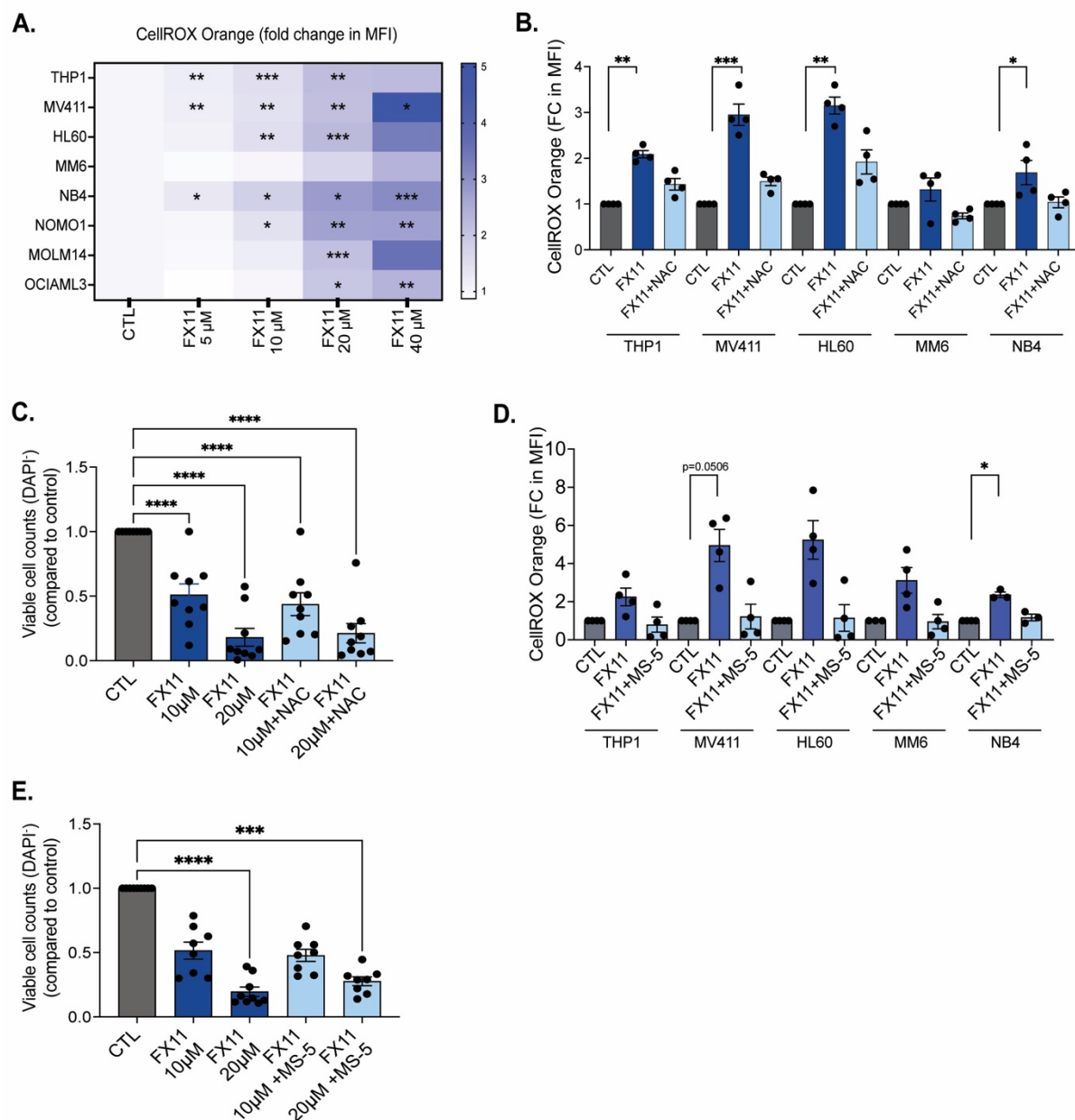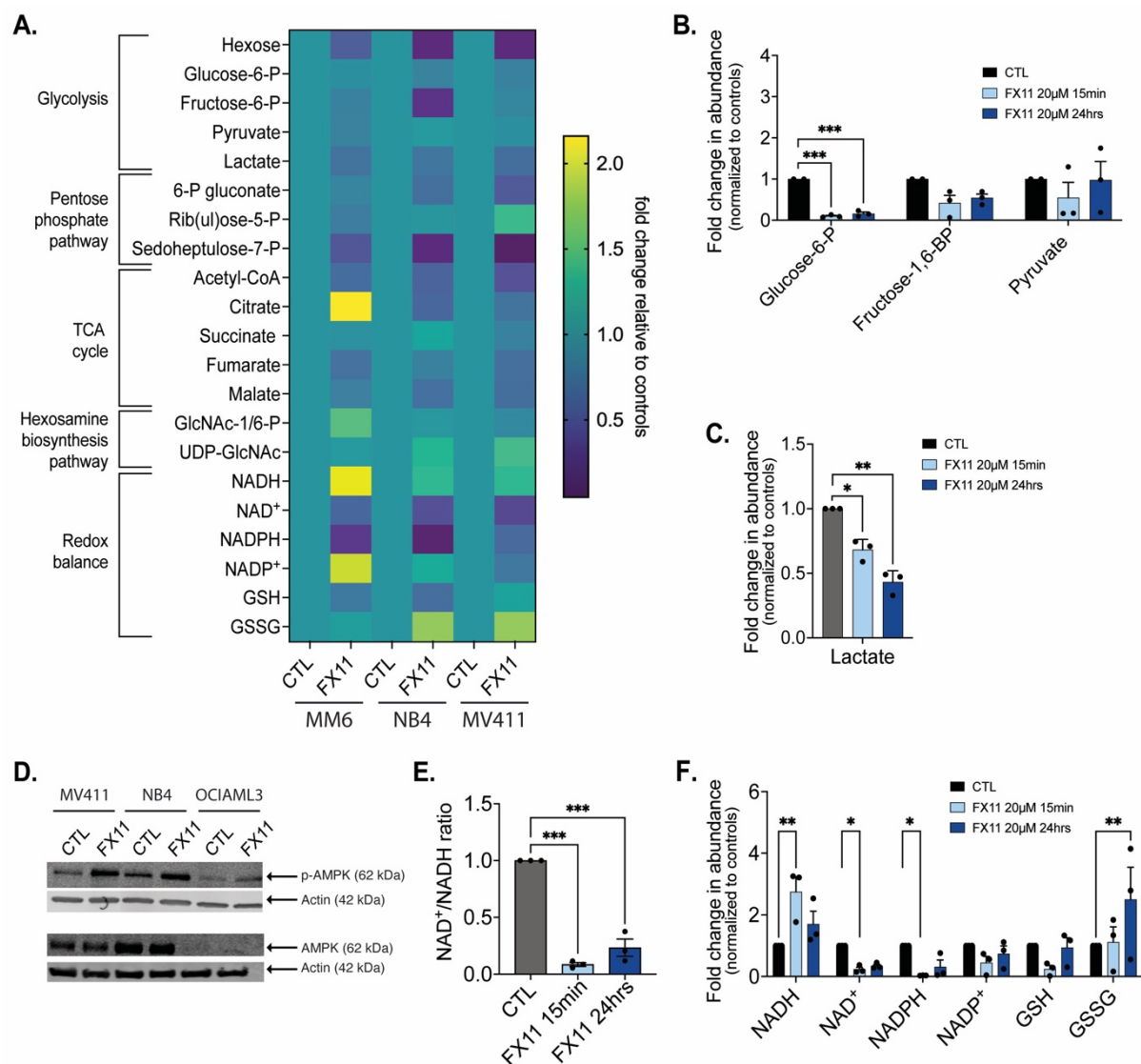789 0.01; ***$p < 0.001$; ns, not significant.

802   **Figures**

803

804   **Figure 1**

805

806

807

808

Figure 2

819 **Figure 3**

820

821

822

823

824

825

826

827

828 **Figure 4**

829

830

831

832

833

834

835

836

837

838
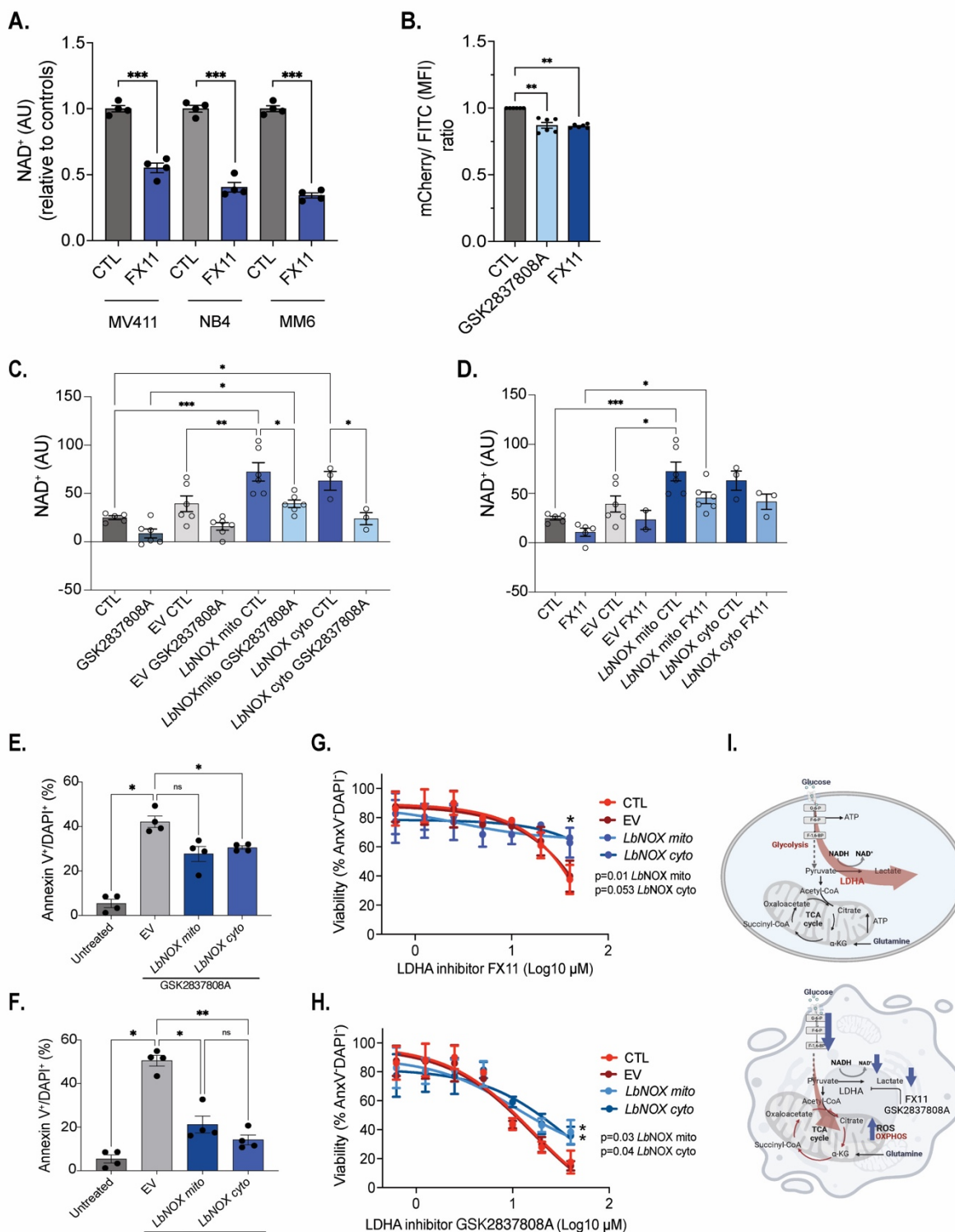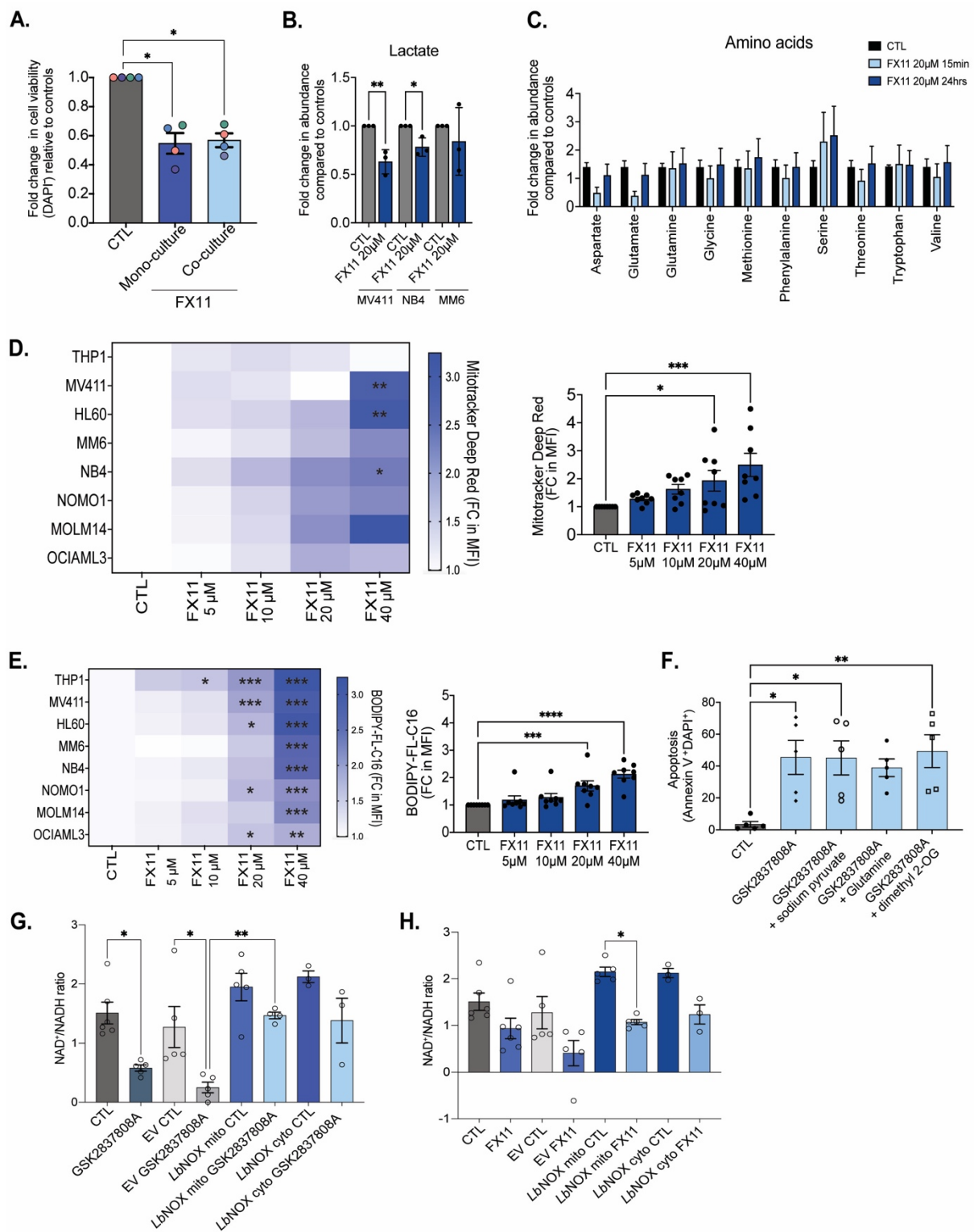
Figure 5

844 **Supplementary Data**

845

846 **Supplementary Figure 1**.

847 **A.** Number of viable (DAPI⁻) cells relative to controls in primary AML patient samples following

848 20 μM FX11 treatment in the presence (co-culture) and absence (mono-culture) of MS-5 cells

849   for 48 hours. Each dot represents a distinct AML sample, as mean of biological triplicates. **B**.

850   Intracellular lactate levels in different AML cell lines after 24 hours of treatment with 20 μM

851   FX11, as measured by LC-MS. Each dot represents a technical replicate. **C**. Relative

852   abundance of amino acids in NB4 cells after 15 minutes and 24 hours of treatment with 20 μM

853   FX11, as measured by LC-MS. Bars show mean ± SEM of biological triplicates. **D**. Heatmap

854   (left panel, per AML cell line tested, data show mean of biological triplicates) and bar graph

855   (right panel, each dot shows a distinct AML cell line) showing the fold change of MitoTracker

856   Deep Red mean fluorescent intensity in AML cell lines exposed to increasing concentrations

857   of FX11 for 24 hours, compared to DMSO treated controls. **E**. Heatmap (left panel, per AML

858   cell line tested, data show mean of biological triplicates) and bar graph (right panel, each dot

859   shows a distinct AML cell line) showing the fold change of BODIPY-FL-C$_{16}$ mean fluorescent

860   intensity in AML cell lines exposed to increasing concentrations of FX11 for 24 hours,

861   compared to DMSO treated controls. **F**. Percentage dead (Annexin V$^+$DAPI$^+$) AML cells

862   treated with 20 μM GSK2837808A alone or with 2 mM sodium pyruvate, 2 mM glutamine or

863   400 μM dimethyl 2-OG (2-oxoglutarate) for 24 hours. Each dot represents a distinct AML cell

864   line, as mean of biological triplicates. **G-H**. Cellular NAD$^+$/NADH ratio in NB4 control cells, NB4

865   cells transduced with an empty vector (EV) and NB4 cells overexpressing a mitochondrial or

866   cytosolic variant of *Lb*NOX, treated with vehicle or 20 μM GSK2837808A (G) or 20 μM FX11

867   (H) for 24 hours, as measured by enzymatic assay. **B**: Student's t test; **A,D,E,F,G,H**: one-way

868   ANOVA for multiple comparisons. All experiments: bars and error bars represent mean ± SEM.

869   *$p < 0.05$; **$p < 0.01$; ***$p < 0.001$; ****$p < 0.0001$.

870

871

872

873

874

Supplementary Table 1: Patient characteristics

Sample ID	Sample information & known mutations
AML1	BCORL1, DNMT3A, NRAS, PTPN11, TET2, U2AF1I
AML2	FLT3-ITD, NPM1, DNMT3A, TP53
AML3	MLL rearrangement
AML4	BCOR, DNMT3A, NRAS, RUNX1, STAG2
AML5	AML (no CD34$^+$ cells)
AML6	KIT, PTPN11, WT1
AML7	NPM1, TET2
AML8	ASXL1 germline
AML9	Chronic neutrophilic leukemia (CNL) with classic activating mutation in CSF3R (CSF3R-T618I).
AML10	Venetoclax resistant AML; FLT3, IDH2, RUNX1, TET2
AML11	FLT3-ITD, NPM1, WT1 frameshift
AML12	DNMT3A, NPM1, WT1
AML13	BRAF, GNAS, JAK2, NRAS, TET2
AML14	DNMT3A, FLT3, NPM1
AML15	CEBPA

875